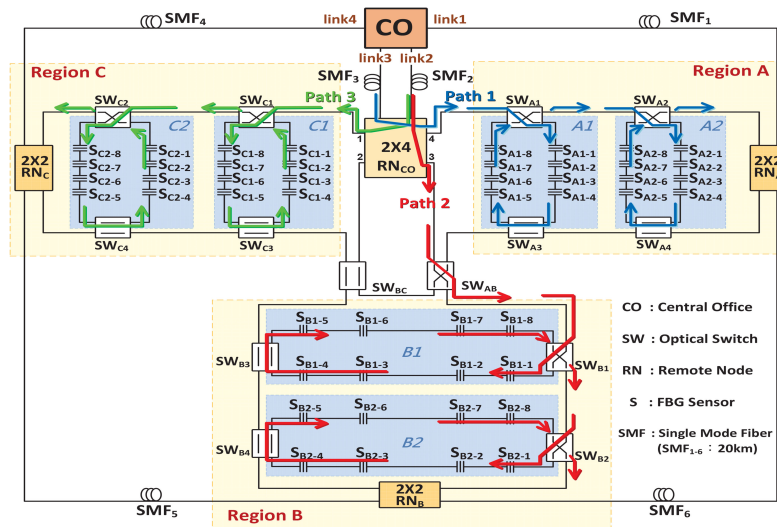


# A Large-Scale Optical Fiber Sensor Network With Reconfigurable Routing Path Functionality

Volume 11, Number 3, June 2019

Ching-Hung Chang  
 Chia-Heng Tsai



DOI: 10.1109/JPHOT.2019.2919196  
 1943-0655 © 2019 IEEE

# A Large-Scale Optical Fiber Sensor Network With Reconfigurable Routing Path Functionality

Ching-Hung Chang  and Chia-Heng Tsai

Department of Electrical Engineering, National Chiayi University, Chiayi 60004, Taiwan

DOI:10.1109/JPHOT.2019.2919196

1943-0655 © 2019 IEEE. Translations and content mining are permitted for academic research only.

Personal use is also permitted, but republication/redistribution requires IEEE permission.

See [http://www.ieee.org/publications\\_standards/publications/rights/index.html](http://www.ieee.org/publications_standards/publications/rights/index.html) for more information.

Manuscript received March 5, 2019; accepted May 23, 2019. Date of publication May 27, 2019; date of current version June 17, 2019. This work was supported by the Ministry of Science and Technology, Taiwan, R.O.C, under Contract MOST 105-2221-E-415-010-MY2 and MOST 107-2221-E-415-009-. Corresponding author: Ching-Hung Chang (e-mail: chchang@mail.nyu.edu.tw).

**Abstract:** A novel large-scale three-layer-ring optical fiber sensor network is proposed with reconfigurable routing functionality. To provide large-scale sensing region as hybrid star-ring architecture and to provide robust self-healing function to deal with large amount of fiber-link failures as mesh architecture, the proposed architecture utilizes optical switches (SW) and new type of remote nodes (RNs) to compose the entire system in three layers. In the first layer, several fiber Bragg grating (FBG) sensors connect each other to compose a sensing subnet. In the second layer, several FBG sensing subnets connect each other by SWs to form the ringed sensing regions. In the third layer, each sensing region connects with central office by RNs. When fiber-link failure occurs in the system, the proposed three-layer-ring architecture can immediately restore the sensing signals by changing the status of the SWs and RNs in the sensing network. According to the simulation results, the proposed three-layer-ring architecture can completely restore the sensing signals when there are up to four break points occurring in a sensing region at the same time. The observed optical spectra of the received optical sensing signals in CO are roughly identical when the proposed architecture has no fiber-link failure or has up to four breakpoints.

**Index Terms:** Optical fiber sensor, fiber Bragg grating (FBG), reconfigurable routing path function, self-healing.

## 1. Introduction

The global warming has a huge impact on the world such as the sea level rising as the polar ice fields thaw and the coastal lands being covered gradually. More than that, it results in abnormal rainstorms, violent volcanic eruption activities and frequent earthquakes all over the world, leading to constant natural disasters, such as landslide, tsunami and debris flow [1]. According to the statistics of IRIS (Incorporated Research Institutions for Seismology), there were almost 3,000 earthquakes above scale 6.0 in the world in the past 20 years (1999-2018) [2]. Under the effect of global warming, the seawater temperature rose year by year, increasing the probability of tropical cyclone indirectly [3], [4]. In addition, improper exploitation of hillsides resulted in earth loss and looseness, which initiated debris flow, reservoir sedimentation and flashflood, not only threatening the residents' lives, but also impacting the economy severely. In view of this, enhancing the detection in these regions where disasters are likely to occur becomes an important work. In order to prevent the damage resulted from natural disasters, the traditional electronic sensor network system came

out. However, such natural disasters as landslide, debris flow and flood often occur in the places far from metropolitan areas and thinly inhabited. The system using traditional electronic observation instruments as sensors shall overcome the power supply problems and the data transmission range constraint. The electronic sensors will have rustiness and short circuit problems in the moist environment. If the cable is exposed to wind, sun or rain in a long period of time, the outer insulating layer will be damaged or flake, there may be electric leakage and sparks. On the contrary, the optical fiber sensing system uses light as transmission medium, the optical fiber acts as the signal transmission channel, the transmission attenuation rate of light in the optical cable is much lower than that in the cable, the transmission distance is longer. In addition, the transmission of light signals in the optical fiber is free from the interference of electromagnetic waves and cross talk, and the high sensitivity can be used for detecting weak signals. Due to these characteristics, optical fiber sensing technology has received great attention and been applied in various fields, such as aerospace industry, medical technology, national defense security, geological hydrology, pipeline monitoring and so on [5]–[7]. The sensors used in the optical fiber sensing system are used fiber Bragg grating (FBG), each FBG sensor can reflect a light signal of specific wavelength, the signals of the other wave bands will penetrate directly, and the reflection wave band of FBG sensor drifts with the temperature change and stress variation of current environment [8]. In addition to sensing temperature and stress changes, FBG can also detect the magnetic, dynamic water pressure, ultrasound and so on [9]–[11]. Based on FBG characteristic, the changes in the sensing environment can be remotely judged according to the feedback signals reflected by FBG sensor, and these data are analyzed to evaluate the probability of accidents, so as to predict natural disasters. Generally, if an optical fiber sensor network is set as tree topology, the central office can use one common trunk fiber in the tree architecture to bridge multiple branch fibers connected with FBG sensors in remote area. This can save the deploying cost and makes the optical fiber sensor network more applicable to remotely sensing harsh environment than the electronic sensor network. Nevertheless, if the optical cable breaks due to a resistless accident, e.g., landslide, debris flow or bridge break, all of the FBG sensors connected after the breakpoint will not feed their sensing signals back to the CO. In order to solve this problem, many optical fiber sensor network structures, such as ring architectures, hybrid architectures and mesh architectures, have been proposed with routing path reconstruction function. The ring architecture is divided into single ring and two-level ring [12]–[15]. The single ring architecture proposed in [12] employs an  $N \times N$  remote node (RN) to connect  $N$  single ring sensing loops, and the architecture proposed in [14] connects multiple annular sensing regions in series, and every annular sensing region is connected by  $2 \times 2$  optical switches. When anyone fiber link lost its connection function, the  $N \times N$  RN in [12] and the optical switch in [14] will provide backup routing path to recover the blocked connection. In parallel with single ring structure, the Two-level ring architecture in [15] is mainly constructed by an outer fiber ring line and an inner fiber ring line, and multiple annular sensing regions are bridged between the inner and outer rings to form the second-order annular loop. By utilizing multiple optical switches to bridge each annular sensing region with the inner and outer rings, the network function can be ensured if the number of breakpoints in the annular sensing regions is less than two. However, the single ring or two-level ring architecture cannot expand the sensing range due to the attenuation of the employed  $N \times N$  RN and optical switches. In order to enlarge the system sensing range, different hybrid sensor network architectures are propose, such as star-ring, star-ring-bus or star-bus-ring architecture [16]–[19]. Due to the combination of different network topologies, the number of available routing path is increased, so their sensing range breaks through the limitations of ring architecture. In comparison to the ring architecture, the hybrid sensor network architecture is relatively free in laying aspect. To further extend the network scale and self-healing functionality, the mesh sensor network architectures are developed [20]–[22]. The architecture can expand freely, the sensing range is maximized, and the routing path is extremely free. However, due to the great quantity of preinstalled optical switches in each bridge point of the mesh network, the increased deploying cost and signal attenuation will limit its application. Furthermore, to accomplish the self-healing function in the mesh-sensor network, a complicate algorithm is required to be developed to reconstruct the routing path.

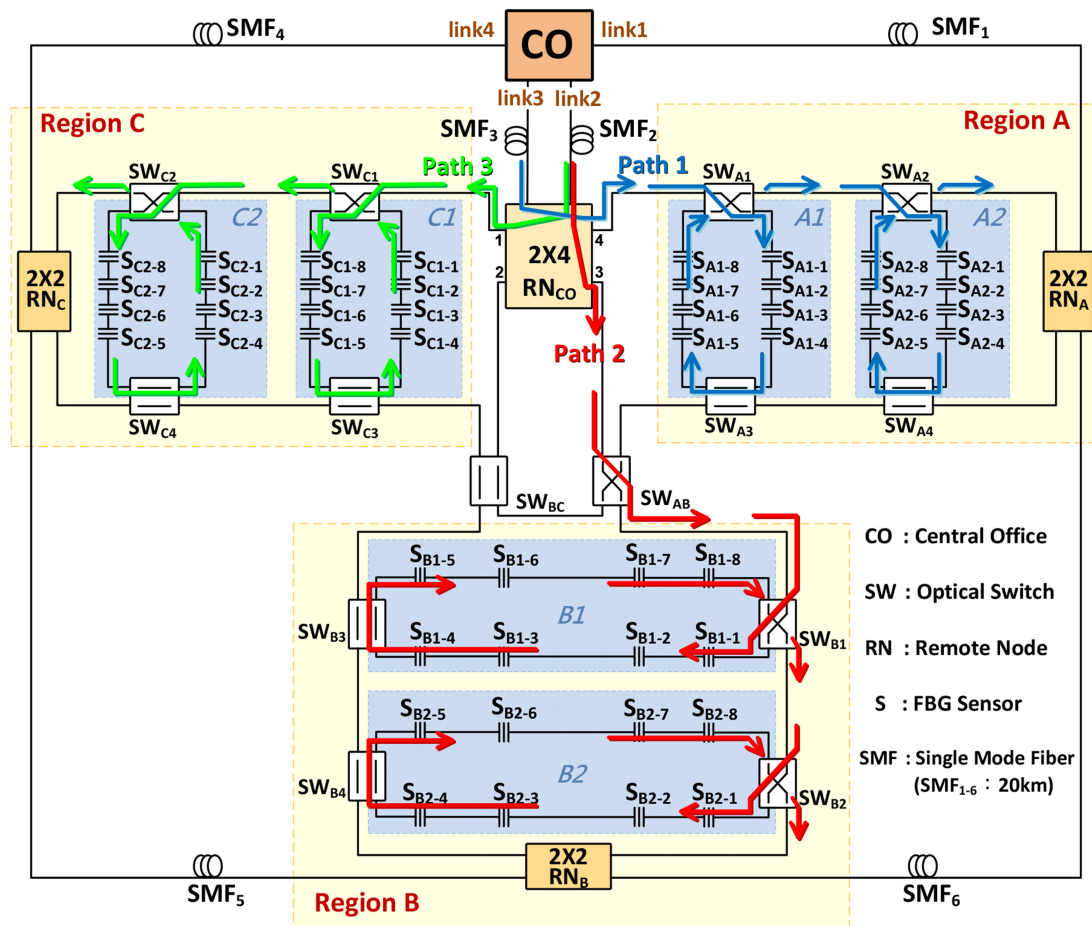


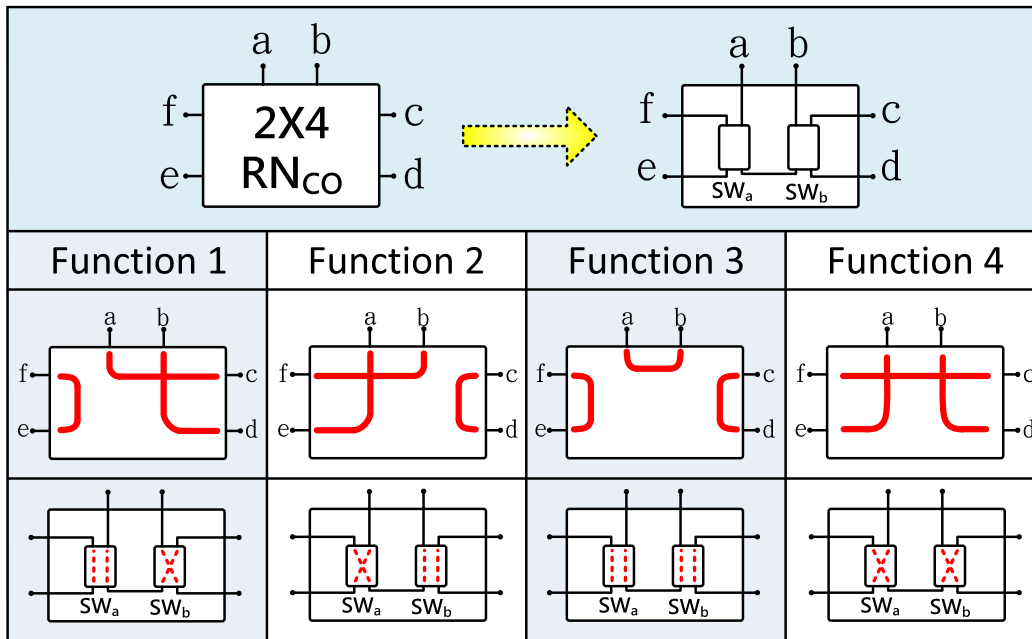
Fig. 1. The proposed three-layer-ring fiber sensor network.

To combine the advancement of the discussed hybrid star-ring, star-ring-bus and mesh sensor network architectures, a three-layer-ring fiber sensor network architecture is proposed and evaluated. In the proposed architecture, the acceptable quantity of fiber breakpoints and sensing range are intermediate between the hybrid and mesh types. In this architecture, adjacent FBG sensors are connected in series to form ring subnetworks, and the subnetworks are connected side by side to compose multiple annular sensing areas according to their geographic locations. Finally, each annular sensing area is connected to the CO based on star and ring topologies. To evaluate the proposed architecture, various network scenarios are developed and simulated by VPItransmissionMaker Optical System. The simulation results validate that when the number of link failure in each sensing area are less than four, the lost sense signals can be obtained again by reconstructing the light routing path. In addition, the number of ring subnetworks in each sensing area can be increased freely, and the number of sensing areas in this architecture can be increased or reduced according to actual demand.

## 2. Proposed Fiber Sensing Network Architecture

The schematic diagram of the proposed three-layer-ring fiber sensor network architecture is shown in Fig. 1. In order to present the operation principle, whole FBG sensors are divided into three sensing regions (*Region A, B, and C*) and are bridged to the CO based on three-layer-ring topology. The first layer of system (*Layer<sub>1st</sub>*) is a small sensing ring subnet consisted of several adjacent FBG

TABLE 1  
 $2 \times 4RN_{CO}$  Architecture and Menu

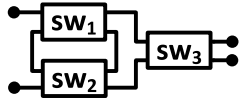
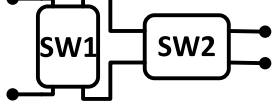
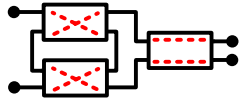
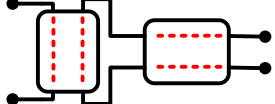
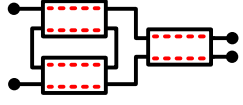
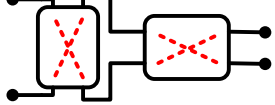
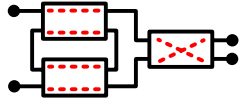
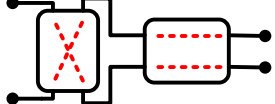


sensors ( $S_s$ ) in each region connected annularly. Taking *Region A* as an example,  $S_{A1-1}$  to  $S_{A1-4}$  and  $S_{A1-5}$  to  $S_{A1-8}$  are connected by optical switches  $SW_{A1}$  and  $SW_{A3}$  to form a sensing ring subnet ( $A1$ ),  $S_{A2-1}$  to  $S_{A2-4}$  and  $S_{A2-5}$  to  $S_{A2-8}$  are connected by optical switches  $SW_{A2}$  and  $SW_{A4}$  to form another sensing ring subnet ( $A2$ ). These sensing ring subnets in the same region are connected in parallel by their optical switches ( $SW_{A1} \sim SW_{A4}$ ), and then connected to the remote node  $2 \times 2RN_A$  of the region to form the *Region A*, i.e., the second layer of this system ( $Layer_{2nd}$ ). In the same manner, in *Region B* and *C*, the  $B1$  and  $B2$  sensing ring subnets of  $S_{B1-1}$  to  $S_{B1-8}$  and  $S_{B2-1}$  to  $S_{B2-8}$  connected in series and the  $C1$  and  $C2$  sensing ring subnets of  $S_{C1-1}$  to  $S_{C1-8}$  and  $S_{C2-1}$  to  $S_{C2-8}$  connected in series will be connected to their RNs ( $2 \times 2RN_B$  and  $2 \times 2RN_C$ ) of each region respectively to form a sensing region. In this transmission system, the  $CO$  and various sensing regions will be connected to form a star and ring topology by the third layer ( $Layer_{3rd}$ ) of system. In this layer, the signal connection consists of two parts. Part 1, the  $CO$  is connected to the RNs ( $RN_A$ ,  $RN_B$  and  $RN_C$ ) outside each sensing region by the single mode fibers ( $SMF_1$ ,  $SMF_4$ ) of *link1* and *link4* to form the peripheral ring loop of  $Layer_{3rd}$ . Part 2, the central remote node ( $2 \times 4RN_{CO}$ ) and two optical switches ( $SW_{AB}$ ,  $SW_{BC}$ ) connect these sensing regions in star and ring topology, and then which are connected to the  $CO$  by single mode fibers ( $SMF_2$ ,  $SMF_3$ ) of *link2* and *link3* to form the inner ring loop of  $Layer_{3rd}$ .

### 3. Simulation Results and Discussion

In the proposal, the  $2 \times 4RN_{CO}$  bridges the  $Layer_{3rd}$  inner ring loop at the adjacency of  $CO$  and each sensing region. In order to route the optical sensing signals from the  $CO$  to various regions flexibly, the  $2 \times 4RN_{CO}$  uses two  $2 \times 2SW$  ( $SW_a$  and  $SW_b$ ) to implement the four routing functions shown in Table 1. In the status of Function 1, the  $SW_a$  and  $SW_b$  are in parallel and cross status respectively, so as to connected the input signals from port  $a$  to port  $c$  ( $a-c$ ), from port  $b$  to port  $d$  ( $b-d$ ), and from port  $e$  to port  $f$  ( $e-f$ ). The signals fed from the  $CO$  will be connected to the right-hand side of  $2 \times 4RN_{CO}$ , e.g., *Region A* and  $SW_{AB}$ . When the  $CO$  is going to deliver sensing signals to *Region C* and  $SW_{BC}$ , the  $2 \times 4RN_{CO}$  will be in the operation mode of Function 2, which is to say,

TABLE 2  
Comparison Between the Proposed  $2 \times 2RN$  and Published  $2 \times 2RN$  Architectures

Function	Published 2X2RN in [15 - 17]	Proposed 2X2RN
<b>2X2RN</b>		
1		
2		
3		

the  $SW_a$  is turned from parallel status into cross status, and the  $SW_b$  is turned from cross status into parallel status, the channels  $a-e$ ,  $b-f$ , and  $c-d$  will be connected up respectively. In addition, when an optical fiber breakpoint occurs, the  $SW_a$  and  $SW_b$  can be set as parallel status or cross status simultaneously, forming the operation modes of Function 3 and Function 4. In these two modes, channels  $a-b$ ,  $c-d$ ,  $e-f$  and  $a-e$ ,  $b-d$ ,  $c-f$  will be connected up respectively.

The structure of the remote node of each sensing region,  $2 \times 2RN_A$ ,  $2 \times 2RN_B$  and  $2 \times 2RN_C$ , is modified from the prototype used in [15]–[17]. Table 2 is the look-up table of internal architectures and functions of the proposed  $2 \times 2RN$  and published  $2 \times 2RN$  in [15]–[17]. According to Table 2, the published  $2 \times 2RN$  consists of three  $2 \times 2SWs$ ; the function of U-status, parallel and cross route modes can be obtained by changing the status of these three  $SWs$ . In terms of reducing the cost and complexity of the  $2 \times 2RN$ , the number of  $SWs$  is reduced from 3 to 2 ( $SW_1$ ,  $SW_2$ ). When the  $SW_1$  and  $SW_2$  are in parallel status,  $RN$  is in U-status mode. If the  $SW_1$  and  $SW_2$  are changed into cross status, the  $RN$  turns into parallel mode. When  $SW_1$  is in cross status and  $SW_2$  is in parallel status, the  $RN$  is in cross mode. Therefore, the simplified  $2 \times 2RN$  in this paper only needs two  $2 \times 2SWs$  to attain the same function of the published  $2 \times 2RN$  in [15]–[17].

In a fiber sensor network, the FBG is used as sensor and its function is to reflect specific optical wavelength. The equation of FBG reflection wavelength ( $\lambda_B$ ) is expressed as:

$$\lambda_B = 2n_{\text{eff}}\Lambda \quad (1)$$

where  $n_{\text{eff}}$  is the effective refractive index of the fiber core of Bragg grating, and  $\Lambda$  is the period of grating [23]. When multiple optical signals fed through the FBGs in  $Layer_{1st}$  of the proposed system, specific optical signal will be reflected by the FBG sensors and then feeds back to the  $CO$  in opposite direction of the downstream routing passway, the signals of other wave bands will penetrate through the FBG sensors directly. When the temperature or stress changes in the sensing region, the grating period of FBG is changed accordingly. According to Eq. (1), the  $\lambda_B$  is proportional to  $\Lambda$ , so that the reflection wavelength of the FBG sensor will offset to longer or shorter wavelength region when the period of grating changes due to the strain or temperature. The relationship of the FBG reflection

wavelength offset with strain variation  $\Delta\varepsilon$  and temperature variation  $\Delta T$  is represented by [24]:

$$\Delta\lambda_B = \lambda_B [(1 - p_e) \Delta\varepsilon + (\alpha + \xi) \Delta T] \quad (2)$$

where  $p_e$  is the photoelastic constant of the FBG,  $\alpha$  is the coefficient of thermal expansion (CTE), and  $\xi$  is the thermo-optic coefficient of FBG. If the temperature is fixed ( $\Delta T = 0$ ), Eq. (2) can be simplified as:

$$\Delta\lambda_B = \lambda_B (1 - p_e) \Delta\varepsilon \quad (3)$$

and the photoelastic constant  $p_e$  is given by [25]:

$$p_e = \frac{n_{\text{eff}}^2}{2} [\rho_{12} - \nu (\rho_{11} + \rho_{12})] \quad (4)$$

where  $p_{11}$  and  $p_{12}$  are the strain tensor, and  $\nu$  is Poisson's ratio of fiber. According to Eq. (3), it is clear that  $\Delta\lambda_B$  is proportional to the  $\Delta\varepsilon$ . Therefore, the larger the variation of stress on FBG is, the larger the offset of reflection wavelength is. Similarly, if the strain is fixed ( $\Delta\varepsilon = 0$ ), Eq. (2) can be simplified as:

$$\Delta\lambda_B = \lambda_B (\alpha + \xi) \Delta T \quad (5)$$

The coefficient of thermal expansion  $\alpha$  and the thermo-optic coefficient  $\xi$  are respectively given by:

$$\alpha = \frac{1}{\Lambda} \frac{d\Lambda}{dT} \quad (6)$$

and

$$\xi = \frac{1}{n_{\text{eff}}} \frac{dn_{\text{eff}}}{dT} \quad (7)$$

According to Eq. (5), it is observed that  $\Delta\lambda_B$  is proportional to  $\Delta T$ . When the temperature of sensing region changes, the FBG reflection wavelength will change accordingly. Based on the aforesaid characteristics, the drift of FBG reflection wavelength can be obtained by comparing the received feedback signal wavelength with the original signal wavelength, so as to remotely analyze the temperature and pressure changes of the sensing regions.

In normal operation of the sensing system proposed in this paper, the CO sends multi-wavelength optical signals via *Path 1* (blue path), *Path 2* (red path) and *Path 3* (green path) in Fig. 1 respectively to Region A, B and C for sensing. Taking sensing Region A as an example, the CO sends out the optical sensing signals containing 16 wavelengths via *link3*, which are routed from  $SMF_3$  and  $2 \times 4RN_{CO}$  to  $SW_{A1}$  of Region A. At this point, the  $2 \times 4RN_{CO}$  is in the status of Function 1,  $SW_{A1}$  and  $SW_{A2}$  in cross status, and  $SW_{A3}$  and  $SW_{A4}$  in parallel status. The wavelengths of the 16 WDM optical sensing signals are set from 1548 nm to 1554 nm, and the wavelength interval between each of them is 0.4 nm (as shown in Fig. 2(a)). When these optical sensing signals enter Region A, they will go through  $S_{A1-1} \sim S_{A1-8}$  of A1 subnet and  $S_{A2-1} \sim S_{A2-8}$  of A2 subnet. If there is no significant change in the environment of A1 and A2 subnet regions, the 16 WDM optical signals will be reflected by these FBG sensors and fed back in the opposite direction of *Path 1* to the CO. The optical spectra of the received feedback signals are shown in Fig. 2(b). In the same manner, the CO can send out sequentially the optical sensing signals via *Path 2* and *Path 3* to detect the status of Region B and Region C. Comparing the spectra of the transmitted and reflected 16 WDM optical signals shown in Fig. 2(a) and (b), each optical sensing signal is properly received with roughly 13.8 dB to 19.5 dB power attenuation due to their routing pathway. It can be expected that once if parts of those optical signals are not received, one or more breakpoint is presented in the system.

To evade the unexpected breakpoint, the proposed system is able to reconfigure the routing path by changing the status of preinstalled optical switches. For example, when the  $SW_{A1}$  of Region A is disconnected from the central remote node ( $2 \times 4RN_{CO}$ ), as shown in Fig. 3(a), the sense signals transmitted via *Path 1* cannot be reflected back normally due to the breakpoint. When the CO dose

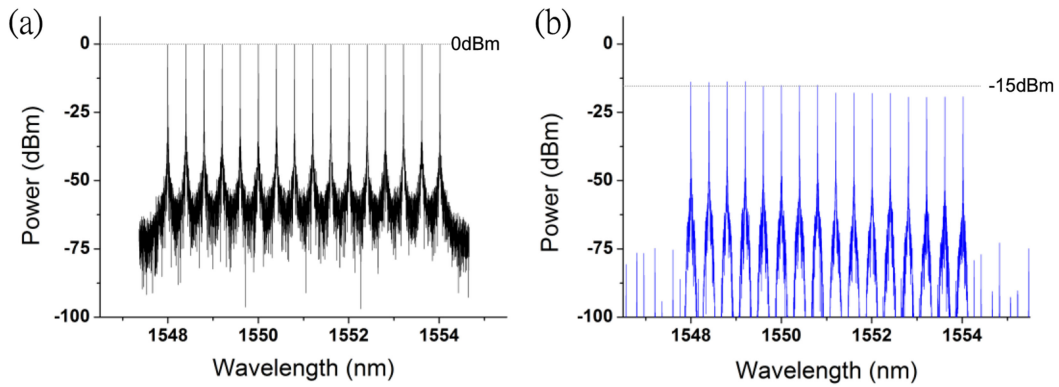


Fig. 2. (a) The spectra of the transmitted WDM signals for the Region A, and (b) the spectra of the received optical signals fed back from the Region A.

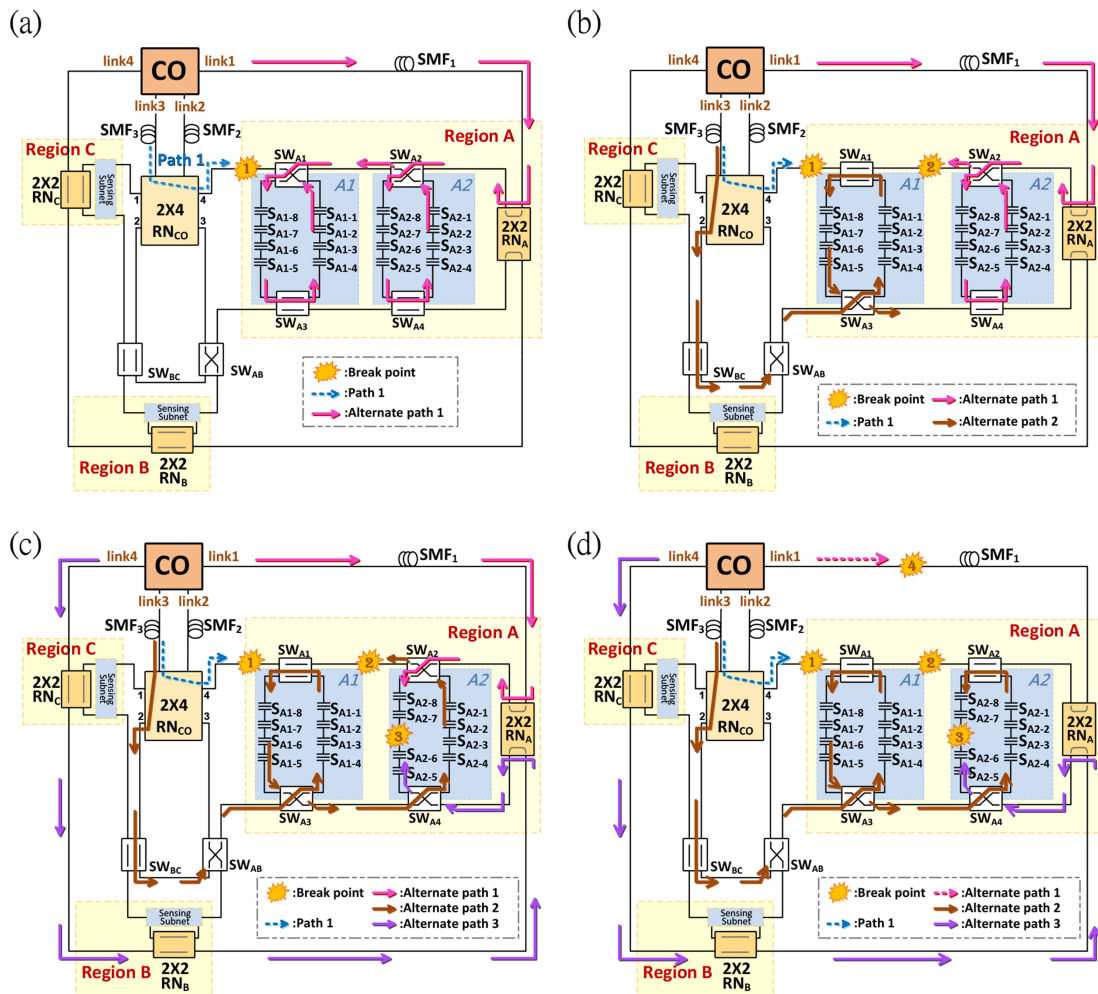


Fig. 3. Schematic diagram of reconfiguring optical route path when Region A of system has (a) 1 breakpoint (b) 2 breakpoints (c) 3 breakpoints and (d) 4 breakpoints.



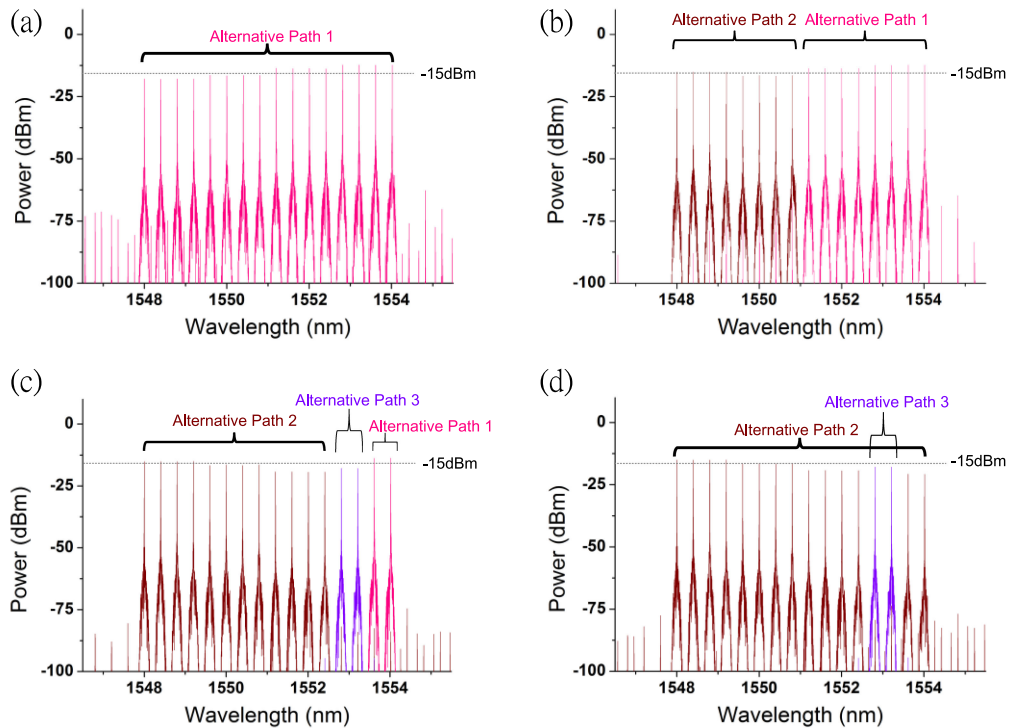


Fig. 4. Optical spectra of the feedback signals received by the *CO* after the optical route path is reconfigured by system when Region *A* of system has (a) 1 breakpoint (b) 2 breakpoints (c) 3 breakpoints (d) 4 breakpoints.

not receive the signals reflected by the FBG sensors in Region *A*, the remote node  $2 \times 2RN_A$  of Region *A* can be modified to the status of Function 1 (U-status route) and the *CO* can alternatively send out WDM optical sensing signals via *link 1* instead of via *link 3*. In this case, the WDM optical sensing signals can be delivered by  $SMF_1$  and  $2 \times 2RN_A$  to each sensor in Region *A*. The route path is called Alternate path 1 (pink line) shown in Fig. 3(a). The spectra of the reflected optical signals received by the *CO* are shown in Fig. 4(a). Comparing the spectra shown in Fig. 2(b) and in Fig. 4(a), the alternative route path only causes slight change in the power of received optical sensing signals. In addition, if the Region *A* has not only one breakpoint, for example, besides the disconnection between the  $2 \times 4RN_{CO}$  and the  $SW_{A1}$ , there is a breakpoint between the  $SW_{A1}$  of *A1* subnet and the  $SW_{A2}$  of *A2* subnet, as shown in Fig. 3(b). At this point, Alternate path 1 only can transmit optical signals to *A2* subnet. In order to sense the status of *A1* subnet, the status of the  $2 \times 4RN_{CO}$  can be changed to Function 2, and the  $SW_{A1}$  and  $SW_{A3}$  of *A1* subnet is changed into parallel status and cross status respectively. In this case, the *CO* can transmit the sense signals to *A1* subnet through the  $2 \times 4RN_{CO}$ ,  $SW_{BC}$ ,  $SW_{AB}$  and  $SW_{A3}$  via Alternate path 2 (brown line). After the optical paths are reconfigured, the spectra of the feedback signals received by the *CO* are shown in Fig. 4(b), in which are slightly better than that of Fig. 4(a). If the system connection status worsens continuously, for example, one more breakpoint in the connection between  $S_{A2-6}$  and  $S_{A2-7}$  as shown in Fig. 3(c), Alternate path 1 will be able to receive the signals of  $S_{A2-7}$  and  $S_{A2-8}$  only, the status of  $S_{A2-1}$  to  $S_{A2-6}$  cannot be detected. At this point, the  $SW_{A4}$  can be converted into cross status, so that the Alternate path 2 is extended through the  $SW_{A4}$  to  $S_{A2-4}$  to  $S_{A2-1}$  of *A2* subnet. To detect the status of residual  $S_{A2-5}$  and  $S_{A2-6}$ , the  $2 \times 2RN_B$  and  $2 \times 2RN_C$  can be set as Function 2 (parallel status), so that the *CO* can transmit the optical signals along the peripheral ring loop of system *Layer<sub>3rd</sub>* via Alternate path 3 (purple line) to detect the  $S_{A2-5}$  and  $S_{A2-6}$  of *A2* subnet. After reconfigured the path, roughly identical spectra of feedback signals are still received by the

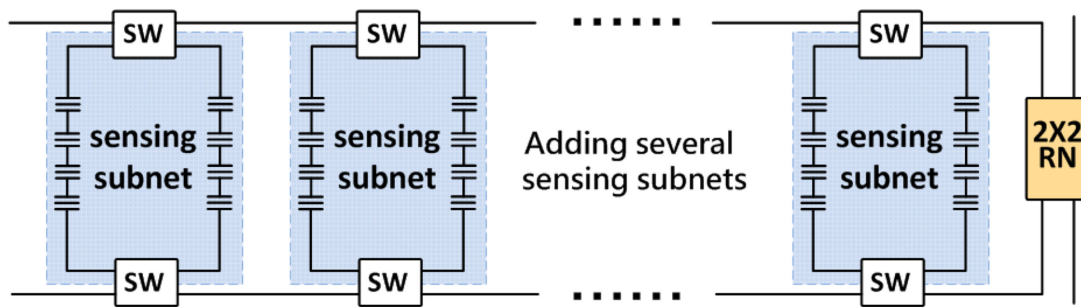


Fig. 5. Schematic diagram of adding sensing subnets in each region.

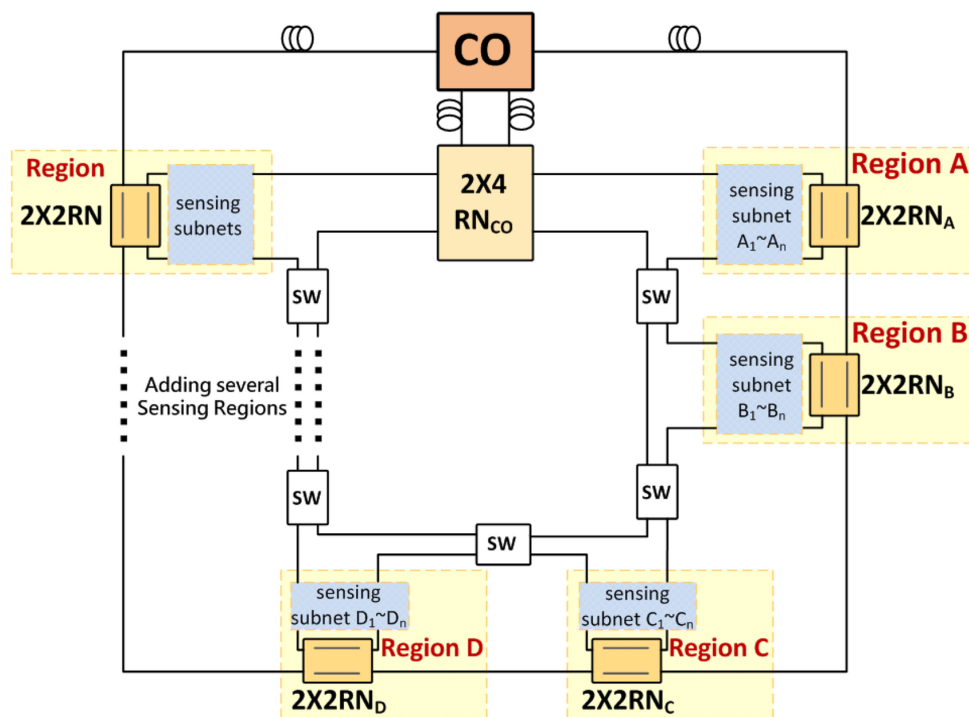


Fig. 6. Schematic diagram of adding sensing regions in the proposed system.

CO, as shown in Fig. 4(c). Under very extraordinary circumstances, if the  $SMF_1$  of *link1* has the fourth breakpoint, Alternate path 1 cannot deliver the signal to the *Region A* successfully, as shown in Fig. 3(d). Only the  $SW_{A2}$  in the *A2* subnet needs to be adjusted. By shifting the  $SW_{A2}$  from cross status into parallel status, the CO will be able to utilize the Alternate path 2 to detect the status of  $S_{A2-7}$  and  $S_{A2-8}$  again. After path reconfiguration, the spectra of feedback signals received by the CO are shown in Fig. 4(d). Similar spectra diagram presented in Fig. 4(a)~Fig. 4(d) demonstrate that the proposed three-layer-ring optical sensor network has great reconfigurable routing path functionality to deal with fiber link failure problem.

In the simulation scenario, only two sensing subnets and three sensing regions are connected in the proposed system. Once some more sensing subnets are needed in each region, the proposed architecture can increase the quantity of *Layer<sub>1st</sub>* subnets and *Layer<sub>2nd</sub>* sensing regions according to different requirements. As shown in Fig. 5, additional sensing subnets can be added in between the original sensing subnets, and connected in parallel by new pairs of SWs. In parallel, extra sensing regions can also be included into the proposed system freely. As presented in Fig. 6, additional

sensing region can be connected to the outer ring of  $Layer_{3rd}$  by extra  $2 \times 2$  RN, and connected to the inner ring of  $Layer_{3rd}$  by a  $2 \times 2$  SW, as long as the  $2 \times 2$  SW is inserted in the inner ring of  $Layer_{3rd}$ , an additional sensing region can be created.

#### 4. Conclusions

Large-scale fiber sensor networks have aroused significant attention to prevent disaster in recent years. To overcome the impact of fiber-link failure and to restore the sensing signals immediately, numbers of fiber sensor networks with reconfigurable routing path have been published. According to the configuration, the topologies those published architecture employed can be divided into three types, e.g., ring, hybrid ring-star-bus and mesh. The ring topology is simple and straightforward, but its sensing area range is limited by self-structure and is difficult to overcome multiple breakpoints in the sensing system. The mesh architecture in turn can provide flexible routing path reconfiguration function to overcome multiple fiber-link failure. Nevertheless, large amount of optical switches and complicated routing path reconfiguration algorithm significantly limit the scale of mesh style fiber sensor networks. To enlarge the network scale size, the hybrid star-ring or star bus architectures are developed but their self-healing function only can used to overcome few breakpoints in their system. To maintain the large-scale characteristic of the hybrid architecture and the effect of the reconfigurable function as in mesh architecture and to cut the hardware cost, a large-scale three-layer-ring fiber sensor network is proposed and evaluated. In the proposal, FBG sensors in each area are firstly grouped as sensing ring subnet and different subnets in the same region are bridged as a sensing region. Consequently, numbers of sensing regions are linked together and are bridged to CO based on same optical switches and new type remote nodes which are optimized from the old type remote node used in the published hybrid fiber sensor networks. By utilizing the optimized remote node in the proposed system, the overall capital expenditure can be reduced and the power budget can be increased to extend the scale of sensing range. Simulation results demonstrate that the proposed three-layer-ring fiber sensor network can deal with up to four breakpoints in each sensing region at the same time by reasonably changing the status of the preinstalled optical switches and remote nodes. The CO will be able to receive roughly identical sensing signals when the optical routing paths are reconfigured to overcome the presented fiber link failures. The proposed architecture reserved flexibility to adjust the number of sensing subnet and sensing region in the system. Simulation results demonstrate that the proposed fiber sensing network can deal with up to four breakpoints in each sensing region at the same time by reasonably changing the status of optical switches and remote nodes.

---

#### References

- [1] B. McGuire, "How climate change triggers earthquakes, tsunamis and volcanoes," *Guardian.*, Oct. 16, 2016. [Online]. Available: <https://www.theguardian.com/world/2016/oct/16/climate-change-triggers-earthquakes-tsunamis-volcanoes>
- [2] "Iris earthquake browser," Incorporated Research Institutions for Seismology (IRIS), 2018. [Online]. Available: <http://ds.iris.edu/ieeb/index.html?format=text&nodata=404&starttime=1999-01-01&endtime=2018-06-11&minmag=6&maxmag=15&orderby=mag-desc&limit=20000&maxlat=89.21&minlat=-89.57&maxlon=180.00&minlon=-180.00&zm=1&mt=ter>
- [3] D. Carrington, "Asian typhoons becoming more intense, study finds," *Guardian.*, Sep. 5, 2016. [Online]. Available: <https://www.theguardian.com/environment/2016/sep/05/asian-typhoons-becoming-more-intense-study-finds>
- [4] E. Kao, "Bigger, badder typhoons and climate change—What's the link?" *South China Morning Post*, Oct. 29, 2017. [Online]. Available: <http://www.scmp.com/news/hong-kong/health-environment/article/2117471/bigger-badder-typhoons-and-climate-change-whats>
- [5] E. Udd, "25 years of structural monitoring using fiber optic sensors," *Proc. SPIE*, vol. 7982, 2011, Art. no. 79820F.
- [6] Q. Rong and X. Qiao, "FBG for oil and gas exploration," *J. Lightw. Technol.*, vol. 37, no. 11, pp. 2502–2515, Jun. 2019.
- [7] K. R. Henken, J. Dankelman, J. J. V. D. Dobbelsteen, L. K. Cheng, and M. S. V. D. Heiden, "Error analysis of FBG-based shape sensors for medical needle tracking," *IEEE/ASME Trans. Mech.*, vol. 19, no. 5, pp. 1523–1531, Oct. 2014.
- [8] A. D. Kersey *et al.*, "Fiber grating sensor," *J. Lightw. Technol.*, vol. 15, no. 8, pp. 1442–1463, Aug. 1997.
- [9] F. Shi, X. Bai, F. Wang, F. Pang, S. Pu, and X. Zeng, "All-fiber magnetic field sensor based on hollow optical fiber and magnetic fluid," *IEEE Sensors J.*, vol. 17, no. 3, pp. 619–622, Feb. 2017.

- [10] P. L. Ko, K. C. Chuang, and C. C. Ma, "A fiber Bragg grating-based thin-film sensor for measuring dynamic water pressure," *IEEE Sensors J.*, vol. 18, no. 18, pp. 7383–7391, Jul. 2018.
- [11] S. Liang *et al.*, "Novel fiber Bragg grating sensing method based on the sidelobe-modulation for ultrasound detection," *J. Lightw. Technol.*, vol. 37, no. 11, pp. 2686–2693, Jun. 2019.
- [12] C. H. Yeh, C. W. Chow, P. C. Wu, and F. G. Tseng, "A simple fiber Bragg grating-based sensor network architecture with self-protecting and monitoring functions," *Sensors (Basel)*, vol. 11, no. 2, pp. 1375–1382, Jan. 2011.
- [13] C. H. Yeh, C. W. Chow, C. H. Wang, F. Y. Shih, Y. F. Wu, and S. Chi, "A simple self-restored fiber Bragg grating (FBG)-based passive sensing ring network," *Meas. Sci. Technol.*, vol. 20, no. 4, Mar. 2009, Art. no. 043001.
- [14] P. C. Peng, H. Y. Tseng, and S. Chi, "A novel fiber-laser-based sensor network with self-healing function," *IEEE Photon. Technol. Lett.*, vol. 15, no. 2, pp. 275–277, Feb. 2003.
- [15] P. C. Peng and K. Y. Huang, "Fiber Bragg grating sensor system with two-level ring architecture," *IEEE Sensors J.*, vol. 9, no. 4, pp. 309–313, Apr. 2009.
- [16] S. T. Kuo, P. C. Peng, J. W. Sun, and M. S. Kao, "A delta-star-based multipoint fiber Bragg grating sensor network," *IEEE Sensors J.*, vol. 11, no. 4, pp. 875–881, Apr. 2011.
- [17] P. C. Peng, J. B. Wang, and K. Y. Huang, "Reliable fiber sensor system with star-ring-bus architecture," *Sensors (Basel)*, vol. 10, no. 5, pp. 4194–205, Apr. 2010.
- [18] P. C. Peng, W. P. Lin, and S. Chi, "Star-bus-ring architecture for fiber Bragg grating sensors," *Japanese J. Appl. Phys.*, vol. 43, no. 10, pp. 7072–7076, Oct. 2004.
- [19] P. C. Peng, H. Y. Tseng, and C. S., "A hybrid star-ring architecture for fiber Bragg grating sensor system," *IEEE Photon. Technol. Lett.*, vol. 15, no. 9, pp. 1270–1272, Sep. 2003.
- [20] H. W. Gu *et al.*, "Hexagonal mesh architecture for large-area multipoint fiber sensor system," *IEEE Photon. Technol. Lett.*, vol. 26, no. 18, pp. 1878–1881, Sep. 2014.
- [21] K. M. Feng, C. Y. Wu, J. H. Yan, C. Y. Lin, and P. C. Peng, "Fiber Bragg grating-based three-dimensional multipoint ring-mesh sensing system with robust self-healing function," *IEEE J. Sel. Topics Quantum Electron.*, vol. 18, no. 5, pp. 1613–1620, Sep. 2012.
- [22] C. Y. Wu, K. M. Feng, P. C. Peng, and C. Y. Lin, "Three-dimensional mesh-based multipoint sensing system with self-healing functionality," *IEEE Photon. Technol. Lett.*, vol. 22, no. 8, pp. 565–567, Apr. 2010.
- [23] D. Kinet, P. Megret, K. W. Goossen, L. Qiu, D. Heider, and C. Caucheteur, "Fiber Bragg grating sensors toward structural health monitoring in composite materials: Challenges and solutions," *Sensors (Basel)*, vol. 14, no. 4, pp. 7394–419, Apr. 2014.
- [24] Z. S. Guo, "Strain and temperature monitoring of asymmetric composite laminate using FBG hybrid sensors," *Structural Health Monitoring*, vol. 6, no. 3, pp. 191–197, Sep. 2007.
- [25] W. W. Morey, G. Meltz, and W. H. Glenn, "Fiber optic Bragg grating sensors," *Proc. SPIE*, vol. 1169, pp. 98–107, 1990.